Lawrence Berkeley National Laboratory

Title
Demonstration of 22-nm half pitch resolution on the SHARP EUV microscope

Permalink
https://escholarship.org/uc/item/2hh232kx

Journal
Journal of Vacuum Science & Technology B Nanotechnology and Microelectronics Materials Processing Measurement and Phenomena, 33(6)

ISSN
2166-2746

Authors
Benk, Markus P
Goldberg, Kenneth A
Wojdyla, Antoine
et al.

Publication Date
2015-11-01

DOI
10.1116/1.4929509

Peer reviewed

Demonstration of 22-nm half pitch resolution on the SHARP EUV microscope

Markus P. Benk,[a] Kenneth A. Goldberg, Antoine Wojdyla, Christopher N. Anderson,
Farhad Salmassi, and Patrick P. Naulleau
Lawrence Berkeley National Laboratory, 1 Cyclotron Rd., Berkeley, California 94720

Michael Kocsis
Inpria Corporation, 2001 NW Monroe Ave., Suite 203, Corvallis, Oregon 97330

The Semiconductor High-Numerical-aperture (NA) Actinic Reticle Review Project (SHARP) is an extreme ultraviolet (EUV)-wavelength, synchrotron-based microscope dedicated to advanced EUV photomask research. The instrument is designed to emulate current and future generations of EUV lithography (EUVL). The performance of the SHARP microscope has been well characterized for its low-NA lenses, emulating imaging in 0.25 and 0.33 NA lithography scanners. Evaluating the resolution of its higher-NA lenses, intended to emulate future generations of EUV lithography, requires a photomask with features down to 22-nm half pitch. The authors fabricated a sample with features down to 20-nm half pitch, exposing a wafer with a standard multilayer coating in the Berkeley microfield exposure tool, and used it to demonstrate real-space imaging down to 22-nm half pitch on the SHARP microscope. The demonstrated performance of SHARP's high-NA zoneplates, together with the extended capabilities of the tool, provide a platform that is available today, suited for research targeted at upcoming generations of EUVL many years into the future. © *2015 American Vacuum Society*. [http://dx.doi.org/10.1116/1.4929509]

I. INTRODUCTION

While extreme ultraviolet (EUV) lithography is moving toward production, EUV masks and mask blanks are still a field of active research.[1–3] Since the tool's commissioning in 2013, Semiconductor High-NA Actinic Reticle Review Project (SHARP) has been used to study a multitude of aspects of EUV mask technology, including defects,[4] their detection[5] and printability,[6] repairs,[6] roughness,[7] impact of nontelecentricity,[8] or multilayer properties.[9]

A detailed discussion of the SHARP microscope and its capabilities can be found in Ref. 10. The microscope features a lossless Fourier synthesis illuminator[11] that allows it to synthesize arbitrary angular source spectra, and user-selectable zoneplate lenses matching the mask-side aperture of current and future generations of EUV lithography. Up to the present day, the tool has primarily been used to emulate imaging in the ASML NXE3100 and 3300 scanners[12,13] with numerical apertures of 0.25 and 0.33. The imaging performance of SHARP is well characterized for its 0.25 and 0.33 4×NA zoneplates.[14]

With EUV getting closer to preproduction and with the availability of the AIMS tools,[15] which will be used for some of the tasks that are currently performed at SHARP, we are focusing our efforts on research toward future aspects of EUVL. This includes emulating pixelated freeform source of the FlexPupil illuminator,[16] available in the 33x0 scanners, source optimization, and imaging at higher numerical aperture. Reference 17 outlines an anamorphic projection optic at 0.55 NA to be used in future ASML 3500 scanners. While the mask-side NA of the 0.33 projection optic is 0.0825, the mask side NA of this tool will be about 0.14 in the *x*-direction. The anamorphic design increases the system magnification in the *y* direction to overcome the constraint of low reflectivity on high-angle reflection from conventional, high-efficiency multilayer mirrors. The anamorphic *x*-direction NA value exceeds SHARP's 0.125-NA zoneplate, which emulates 0.5-NA projection optics at 4× demagnification, but it stays below its 0.156 NA zoneplate, which is the highest NA currently available in SHARP.

In order to emulate an anamorphic projection optic at 0.55 NA, we have designed a zoneplate with matching mask-side NA of 0.1375 NA in the *x*-direction and 0.0688 NA in *y*. As a single optical element, this zoneplate cannot provide true anamorphic imaging (i.e., different magnifications in the two directions), but SHARP's digital image sensor makes it possible to effectively compress the image in one dimension and thereby emulate anamorphic imaging.

In order to assure the performance of this new, planned optical element, we study the performance of SHARP's existing high-NA zoneplates. These zoneplates have a higher resolution and testing them therefore requires the use of a photomask with features considerably smaller than photomasks designed for the current generation of 0.33-NA lithography scanners. In order to perform the experiment, we fabricated a target with dense line sizes down to 20-nm half pitch (hp). Unless noted otherwise, all feature sizes given in this article refer to actual size at the target, as indicated by the term *target scale*.

II. TARGET FABRICATION

EUV photomasks are usually patterned by electron-beam lithography. Aiming at a quicker and more economical

a)Electronic mail: mpbenk@lbl.gov

fabrication at small size scales, we used EUV lithography to print resolution test patterns on a multilayer-coated silicon wafer. The resulting wafers can be attached to standard EUV mask blanks, for imaging in SHARP. We refer to these wafer-masks as the *target*. They begin as wafers printed in the Microfield exposure tool (MET), and then they become the *mask* imaged in SHARP.

Forty layer pairs of 6.95-nm molybdenum and silicon were deposited on a 100-mm diameter, 500-μm-thick silicon wafer using DC magnetron sputtering. The wafer was primed with hexamethyldisilazane to promote resist adhesion, and the photoresist was spin-coated directly onto the top layer. No capping layer or absorber was used.

A. Photoresist

The target was fabricated using the metal-oxide based negative-tone photoresist YA70BA from Inpria. A resolution of 10 nm with 1.7 nm line width roughness at 13.5-nm wavelength has been demonstrated for this material at the Paul Scherrer Institute.[18] The resist was chosen because of its high absorbance of approximately $20\,\mu m^{-1}$ compared to conventional polyhydroxystyrene based resists with an absorbance in the range of $4-5\,\mu m^{-1}$. A 30-nm layer of resist was used. Accordingly, the transmission of the resist for EUV is 30% on a double pass, providing a contrast of 54% between the clear multilayer and the absorber. In this calculation, it is assumed that the transmission of the resist is identical before and after developing. In practice, the thickness of the resist layer is reduced after development but the density of metal oxide is increased at the same time. The relatively high contrast between resist and clear multilayer regions allows the use of developed resist pattern as a target pattern without the additional processing steps of depositing an absorber layer and etching it to transfer the resist pattern. Compared to a EUV mask with a tantalum nitride absorber, the contrast of the target is significantly lower, but the approach enabled the production of a target that can be used for resolution tests down to 20-nm hp at the target, at a fraction of the cost and effort of using conventional mask-patterning processes.

B. Exposure

The wafer was patterned in the Berkeley microfield exposure tool (BMET).[11] The BMET is a 0.3 NA, EUV microlithography tool situated on an undulator beamline at the Advanced Light Source at Lawrence Berkeley National Laboratory. The BMET is used for research in key areas of EUV lithography such as photoresists, processing, and photomasks. A resolution of down to 14-nm hp at the wafer has been demonstrated with the BMET.[19] Imaging at 5×-demagnification, the tool has a well-corrected image field of $600 \times 200\,\mu m^2$.

A standard MET test pattern was printed on the wafer from the *bright field* (absorber features on clear multilayer) and from the *dark field* (primarily absorber, with multilayer features) thus producing bright-field patterns and dark-field patterns used in SHARP. The patterns include a range of

vertical lines used in these experiments. Multiple copies of both fields were printed on the wafer, building focus-exposure matrices. The wafer was developed and inspected in a scanning electron microscope (SEM), and the fields with the highest fidelity were selected for use. Figure 1(a) shows an SEM image of a region with 28-nm hp (target scale) horizontal lines from the dark field. The pattern in this field has printed at the correct critical dimension without defects. There are a large number of ∼10-nm particles bound to the surface, mainly on the clear regions. Figure 1(b) shows a region with 22-nm hp (target scale) horizontal lines from the bright field, which is the smallest half pitch that SHARP is expected to resolve. The pattern is well resolved. The SEM image indicates that there may be some traces of resist left on the multilayer surface between the lines.

III. RESOLUTION LIMITS OF THE SHARP MICROSCOPE

In addition to its 0.25 and 0.33 4×NA zoneplates, SHARP is equipped with 0.5 and 0.625 4×NA. The latter optics are for studying imaging at higher mask-side NA and increased chief-ray angle (CRA), relevant to possible, future generations of EUV lithography. Current EUV scanners use a chief ray angle of 6°. Wider cones of light, occurring at higher mask-side NA values require an increased chief ray
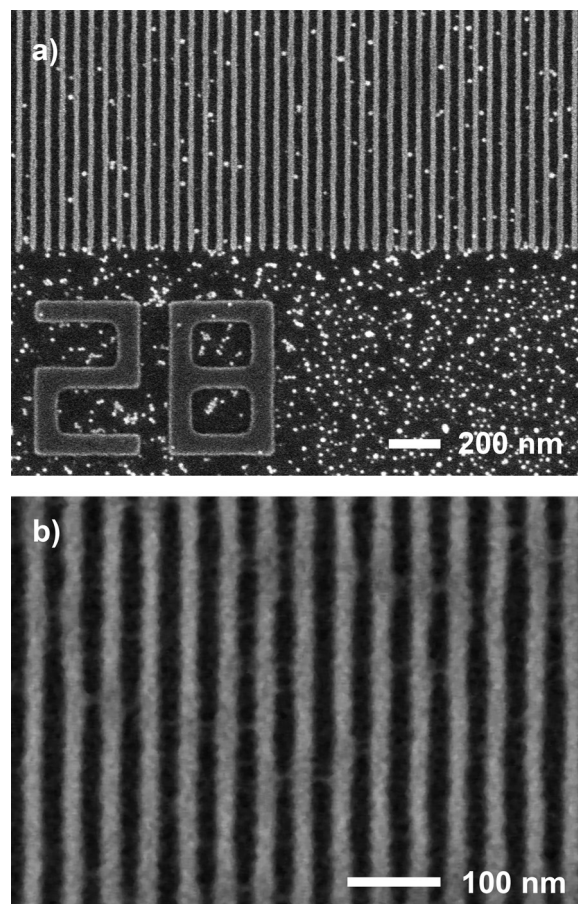

FIG. 1. SEM images, showing (a) 28-nm hp lines (target scale) from the dark field, and (b) 22-nm hp lines (target scale) from the bright field.

TABLE I. Target-scale half-pitch resolution of SHARP's high-NA zoneplates.

	R_C (nm) (coherent)	R_R (nm) (incoherent)	R_L (nm) (dipole)
0.5 4×NA	54	33	27
0.625 4×NA	44	26	22

angle: the 0.5 4×NA zoneplate is designed for 8° CRA and the 0.625 4×NA zoneplate is designed for 10° CRA.

Wavelength and numerical aperture are the primary parameters defining the resolution of an imaging system, yet the illumination coherence properties are equivalently crucial. The data for this study were recorded using three different illumination settings, explained in Sec. IV. For each illumination, there is a corresponding resolution limit. The resolution limit R_C for coherent illumination is

$$R_C = \frac{\lambda}{\text{NA}}. \tag{1}$$

For incoherent illumination, the widely used Rayleigh resolution limit R_R states

$$R_R = \frac{0.61\,\lambda}{\text{NA}}. \tag{2}$$

Using extreme dipole illumination for imaging dense lines, the resolution limit R_L is

$$R_L = \frac{0.5\,\lambda}{\text{NA}}. \tag{3}$$

Equations (1)–(3) correspond to one full cycle (pitch). Half-pitch resolutions are by a factor two smaller accordingly. Table I shows the half-pitch resolution of SHARP's 0.5 and 0.625 4×NA zoneplates for the three resolution limits. Resolution is expected to reach 22-nm hp at the target for the 0.625 4×NA zoneplate with extreme dipole illumination. This corresponds to less than 5.5-nm hp on the wafer side of an EUVL scanner with 4× demagnification.

IV. RESULTS AND DISCUSSION

Vertical dense lines from the dark field were imaged through-pitch in the SHARP microscope. The data were recorded with the 0.5 and 0.625 4×NA zoneplates, using coherent, incoherent, and extreme dipole illumination. Feature sizes range from 100 to 22-nm hp (target scale). Coherent illumination refers to an illumination partial

coherence σ value below 0.01. For incoherent illumination, σ is larger than 0.95. For extreme dipole illumination, the poles have an offset of 0.98 σ and a radius of 0.01 σ. Figure 2 shows pupil diagrams (i.e., angular spectra) for the three illuminations used. The black area represents the extent of the circular pupil. The illuminated angles are shown in white. Note that the poles of the coherent and extreme dipole illumination are magnified for visibility.

A. Base contrast of the target

Figure 3(a) shows an image of 100-nm hp (target scale) horizontal lines and a 1.5-μm-wide border next to the field. The image was recorded with coherent illumination. The bright regions are clear multilayer. In the dark regions, photoresist covers the multilayer. A cross-section plot, taken from the boxed region in Fig. 3(a) and vertically averaged over 80 pixels (864 nm), is shown in Fig. 3(b). The background level of the CCD is calculated from a shadowed region of the image. After background subtraction, the intensity is normalized to unity at the bright border. The intensity in the dark region is approximately 35% due to the finite transmission of the photoresist. From the absorbance alone, the contrast is expected to be 48%. However, the modulation of the 100-nm hp lines is significantly higher, owing to a

FIG. 3. (a) SHARP image of 100-nm hp lines (target scale) and 1.5-μm wide border, and (b) cross-section plot, vertically averaged over 80 pixels (864 nm), taken from the boxed region in (a).
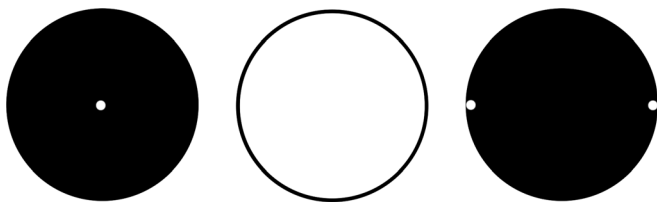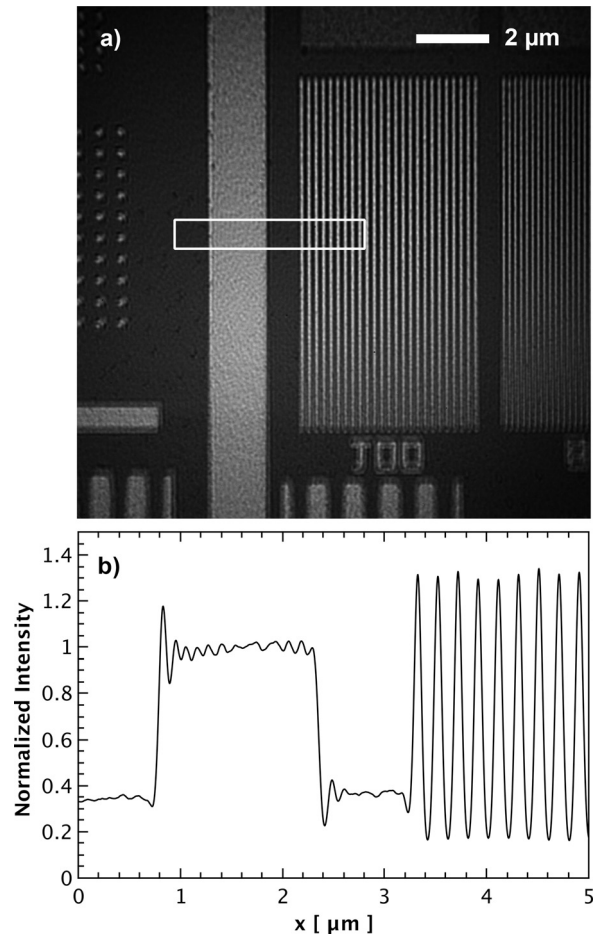

FIG. 2. Pupil diagrams (i.e., angular spectra) of the three illuminations used: coherent illumination (left), incoherent illumination (center), and extreme dipole illumination (right).
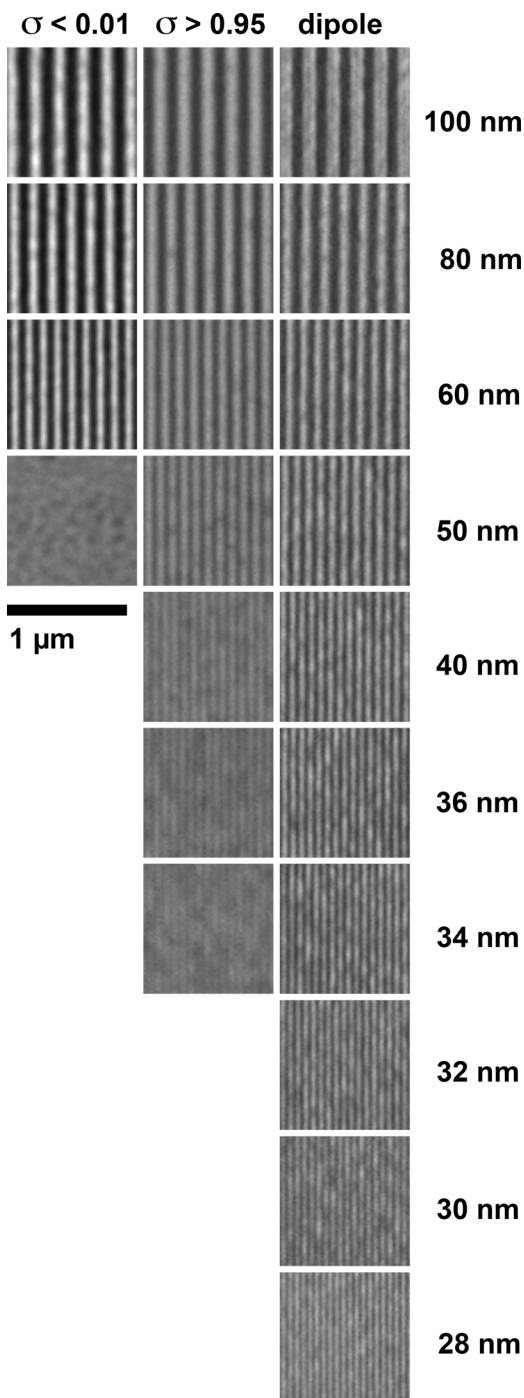
σ < 0.01   σ > 0.95   dipole

FIG. 4. Image details of dense vertical lines through pitch, recorded with the 0.5 4×NA zoneplate using coherent, incoherent, and extreme dipole illumination. Line sizes are half-pitch at target scale.

phase shift of the light transmitted through the photoresist layer, in a double-pass geometry. Interference of light from the clear region and photoresist produces 80% modulation and increased "ringing" at the edges of the clear border.

B. Imaging results

Imaging results from SHARP's high-NA zoneplates with a state-of-the-art EUV mask down to 62 nm hp (mask scale) are published in Ref. 14. Contrast levels of 95% were
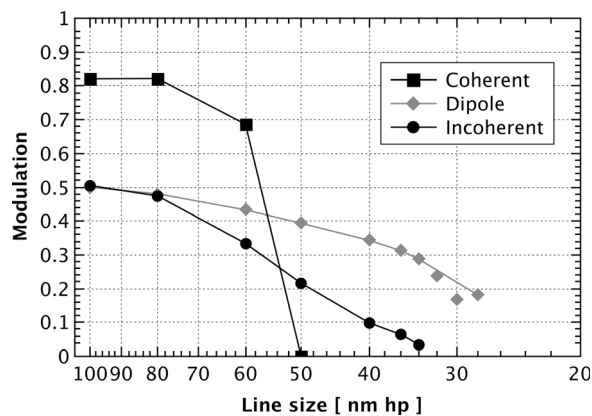
FIG. 5. Contrast curves through pitch for the image data from Fig. 4. Line sizes are half-pitch at target scale.

achieved with the high-NA lenses and a partial coherence of $\sigma = 0.8$. The purpose of this study is to provide data for pitches smaller than are present on today's EUV masks and demonstrate SHARP's capabilities to extend EUV imaging several generations into the future. Due to the different character of the sample, and the relative thinness of the photoresist absorber layer, the modulation and signal-to-noise ratio are lower here.

Figure 4 shows details of dense vertical lines, imaged through pitch, recorded with the 0.5 4×NA zoneplate, using coherent, incoherent, and extreme dipole illumination. The magnification gives an effective pixel spacing of 10.8 nm/pixel. The individual fields correspond to 100×100 pixels on the sensor (1.08–μm width). The data are normalized across the fields to an identical integrated number of counts. To facilitate comparison, all fields shown have the same intensity scaling with the CCD background being black and the brightest pixel in the field with the highest contrast (100-nm hp, coherent) being white. The fields are enlarged for increased visibility of the smallest pitches. The data for the 0.625 4×NA zoneplate, shown in Fig. 6, are processed the same way. With this zoneplate the effective pixel spacing is 8.25 nm/pixel. Figure 5 shows contrast curves through pitch for the image data from Fig. 4. Contrast curves for the data from Fig. 6, recorded with the 0.625 4×NA zoneplate, are shown in Fig. 7. The contrast curves are represented by straight lines connecting the data points in the graphs. The extreme dipole images have higher relative uncertainty due to the difficulty of aligning the system precisely in this extreme condition, and the small usable field of view that results. In the extreme dipole curves, the connecting lines are drawn skipping a few of the data points where the measured modulation is lower than the surrounding points.

To determine contrast, the data were vertically averaged across 100 rows, to reduce noise. The modulation was calculated for each line individually and then averaged. The line-to-line variation in the modulation across the fields has a standard deviation below 2.5 percentage points, typically one percentage point.

The expected base contrast of the target is approximately 50%, and for both zoneplates, the contrast curves for
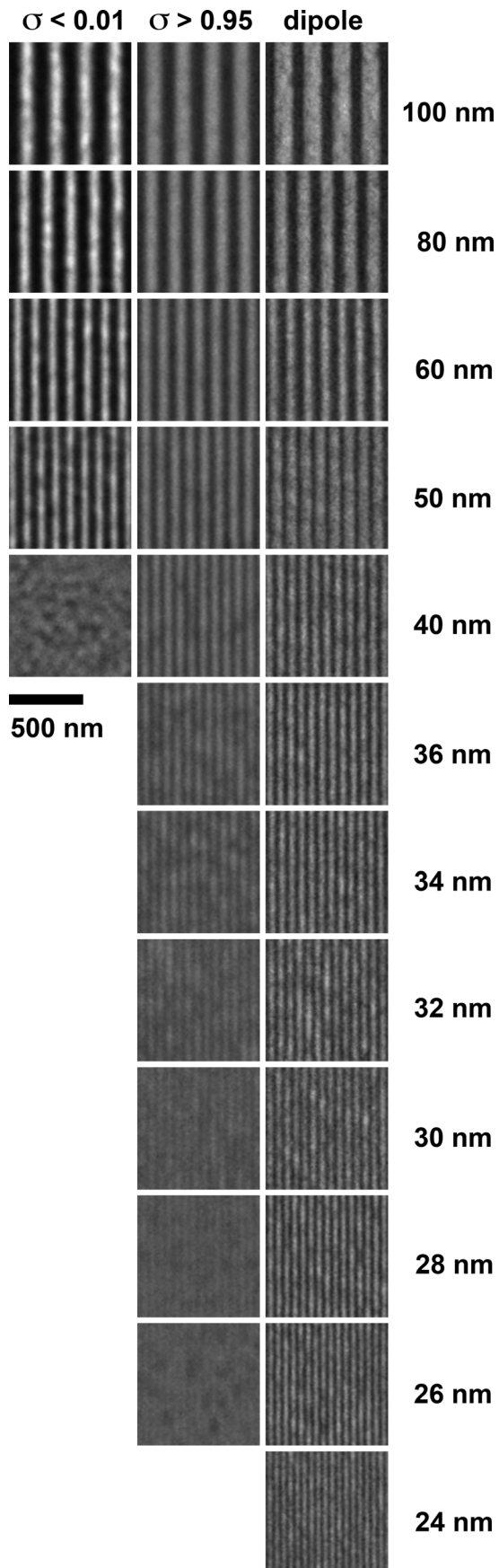
σ < 0.01   σ > 0.95   dipole

100 nm

80 nm

60 nm

50 nm

500 nm

40 nm

36 nm

34 nm

32 nm

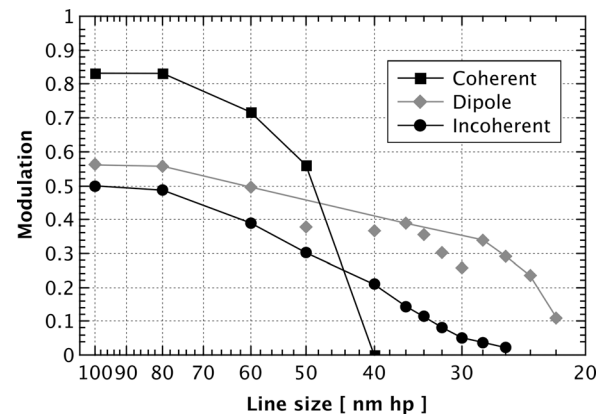30 nm

28 nm

26 nm

24 nm

FIG. 7. Contrast curves through pitch for the image data from Fig. 6. Line sizes are half-pitch at target scale.

incoherent illumination start at 0.5 for the largest feature sizes. Modulation decreases toward smaller pitches. An ideal incoherent imaging system has a modulation transfer of 9% at the Rayleigh resolution limit. From a target with a base contrast of 0.5, a modulation of only 4.5% is expected. The data recorded with the 0.625 4×NA zoneplate has a modulation of 2.2% at 26-nm hp (target scale), right at the Rayleigh limit. For the 0.5 4×NA zoneplate, the modulation at the smallest half pitch above the Rayleigh limit (34 nm at the target) is 3.5%.

The phase shift occurring in the photoresist layer increases the modulation with coherent illumination. For both zoneplates, 84% modulation is observed at 100-nm hp. With coherent illumination, the modulation stays well above that of incoherent illumination and dipole illumination. At the coherent resolution limit, the modulation steeply drops to zero.

With the 0.5 4×NA zoneplate, incoherent and dipole illumination show 50% modulation at 100 nm hp. All feature sizes discussed here are in the scale of the target. For the 0.625 4×NA zoneplate, incoherent illumination produces 50% modulation, while for dipole illumination the modulation is 56%. For both zoneplates, dipole illumination provides higher modulation than incoherent illumination. With
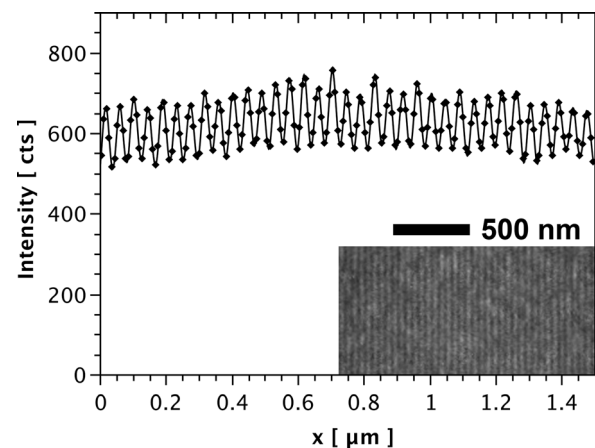

FIG. 6. Image details of dense vertical lines through pitch, recorded with the 0.625 4×NA zoneplate using coherent, incoherent, and extreme dipole illumination. Line sizes are half-pitch at target scale.

FIG. 8. Image detail of 22-nm hp lines (target scale), imaged with the 0.625 4×NA zoneplate and cross-section plot of this data, vertically averaged over 100 pixels covering 1.5 μm.

dipole illumination, the lines are resolved down to the smallest pitch above the resolution limit for both NAs. Modulation is 17% at 28-nm hp for the 0.5 4×NA zoneplate and 11% at 22-nm hp for the 0.625 4×NA zoneplate. The 22-nm data are not included in Fig. 6. Figure 8 shows a 200 × 100-pixel region (1.65 × 0.825 μm^2) with 22-nm hp lines, imaged with the 0.625 4×NA lens, and a cross-section plot of the 22-nm hp lines over 1.5 μm. The graph shows the individual data points (pixel values) and a cubic interpolation of the data. The variation of intensity across the data results from the extreme dipole illumination. In the center of the image, equal amounts of zero-order light from both poles are collected by the zoneplate. Moving off the image center, zero-order light from the opposite side is partially clipped by the aperture causing the intensity in the image to roll off. Pattern imperfections and substrate roughness are two prominent contributors to small-scale variation in intensity and line-to line variation in modulation at this small half pitch.

V. SUMMARY AND OUTLOOK

The SHARP microscope is designed to support advanced photomask research many generations into the future of EUV lithography. The instrument is upgraded frequently to make emerging technologies available in order to study concepts envisioned for future nodes.

Features smaller than approximately 50 nm hp (mask scale) are not present on EUV masks used with current generations of EUV lithography. We have fabricated an ultra-high resolution test pattern mask with features down to 20-nm hp to use with SHARP's high-NA zoneplates. Printing the pattern on a multilayer-coated silicon wafer in the Berkeley MET and using metal-oxide based photoresist directly, as an absorber, is a fast and economical approach to achieve the required feature size. With this target, we have demonstrated real-space imaging down to 22 nm hp (target scale), on the SHARP microscope. This result shows that SHARP's high-NA zoneplates can reach their nominal resolution limits. A next-generation, high-NA zoneplate for SHARP, matching the mask-side NA of an anamorphic projection optic at 0.55 NA, is currently in production and will be available soon. The high-NA zoneplates together with the ability of the instrument to control the angular spectrum of the source to match the illumination used in current and future EUV scanners confirms SHARP's readiness for photomask research at future EUV production nodes.

[1]C.-J. Kim et al., Proc. SPIE **9235**, 92351L (2014).
[2]K. Takai, K. Murano, T. Kamo, Y. Morikawa, and N. Hayashi, Proc. SPIE **9235**, 923515 (2014).
[3]A. O. Antohe, P. Kearney, M. Godwin, L. He, A. J. Kadaksham, F. Goodwin, A. Weaver, A. Hayes, and S. Trigg, Proc. SPIE **9048**, 90480H (2014).
[4]E. Gallagher, A. Wagner, M. Lawliss, G. McIntyre, K. Seki, T. Isogawa, and S. Nash, Proc. SPIE **9256**, 92560K (2014).
[5]Y.-G. Wang et al., Proc. SPIE **9422**, 94221C (2015).
[6]M. Lawliss, E. Gallagher, M. Hibbs, K. Seki, T. Isogawa, T. Robinson, and J. LeClaire, Proc. SPIE **9235**, 923516 (2014).
[7]P.-Y. Yan, G. Zhang, E. M. Gullikson, K. A. Goldberg, and M. P. Benk, Proc. SPIE **9422**, 94220J (2015).
[8]S. Raghunathan et al., J. Vac. Sci. Technol. B **32**, 06F801 (2014).
[9]V. Philipsen, E. Hendrickx, E. Verduijn, S. Raghunathan, O. Wood, V. Soltwisch, F. Scholze, N. Davydova, and P. Mangat, Proc. SPIE **9235**, 92350J (2014).
[10]K. A. Goldberg et al., Proc. SPIE **9048**, 90480Y (2014).
[11]P. P. Naulleau, K. A. Goldberg, P. Batson, J. Bokor, P. Denham, and S. Rekawa, Appl. Opt. **42**(5), 820–826 (2003).
[12]R. Peeters et al., Proc. SPIE **8679**, 86791F (2013).
[13]R. Peeters et al., Proc. SPIE **9048**, 90481J (2014).
[14]K. A. Goldberg, M. P. Benk, A. Wojdyla, D. G. Johnson, and A. P. Donoghue, Proc. SPIE **9422**, 94221A (2015).
[15]M. R. Weiss, D. Hellweg, M. Koch, J. H. Peters, S. Perlitz, A. Garetto, K. Magnusson, R. Capelli, and V. Jindal, Proc. SPIE **9422**, 942219 (2015).
[16]X. Liu et al., Proc. SPIE **9048**, 90480Q (2014).
[17]B. Kneer, S. Migura, W. Kaiser, J. T. Neumann, and J. van Schoot, Proc. SPIE **9422**, 94221G (2015).
[18]A. Grenville et al., Proc. SPIE **9425**, 94250S (2015).
[19]P. Naulleau et al., Proc. SPIE **7636**, 76361J (2010).